Constraining self-organizing map facies analysis with stratigraphy: An approach to increase the credibility in automatic seismic facies classification

Tao Zhao[1], Fangyu Li[1], and Kurt J. Marfurt[1]

Abstract

Pattern recognition-based seismic facies analysis techniques are commonly used in modern quantitative seismic interpretation. However, interpreters often treat techniques such as artificial neural networks and self-organizing maps (SOMs) as a "black box" that somehow correlates a suite of attributes to a desired geomorphological or geomechanical facies. Even when the statistical correlations are good, the inability to explain such correlations through principles of geology or physics results in suspicion of the results. The most common multiattribute facies analysis begins by correlating a suite of candidate attributes to a desired output, keeping those that correlate best for subsequent analysis. The analysis then takes place in attribute space rather than (x, y, and z) space, removing spatial trends often observed by interpreters. We add a stratigraphy layering component to a SOM model that attempts to preserve the intersample relation along the vertical axis. Specifically, we use a mode decomposition algorithm to capture the sedimentary cycle pattern as an "attribute." If we correlate this attribute to the training data, it will favor SOM facies maps that follow stratigraphy. We apply this workflow to a Barnett Shale data set and find that the constrained SOM facies map shows layers that are easily overlooked on traditional unconstrained SOM facies map.

Introduction

Skilled seismic interpreters identify seismic facies by examining spatial variations in seismic reflection amplitude, phase, frequency, continuity, and orientation. Modern seismic attributes and impedance inversion algorithms quantify the local variation of these reflectors voxel by voxel, allowing them to be statistically analyzed by a computer. Zhao et al. (2015) review some of the more commonly used supervised and unsupervised seismic facies classification techniques, such as principal component analysis (PCA), k-means classification, self-organizing maps (SOMs), generative topographic mapping, artificial neural networks, and support vector machines. In general, unsupervised classification techniques are solely driven by the input data, whereas supervised techniques incorporate external control provided either by wells or as data labels defined by the interpreter. In either case, validation of the results is critical to gaining confidence in the prediction. When there is a great deal of well control or interpreter-generated labels (geomorphological/petrophysical facies), statistical validation may be sufficient. However, when the well control is limited or the interpreter is suspect, correlation to well-accepted geologic and petrophysical models provides added confidence. In a conventional reservoir, such a correlation may be that of a gas-sand facies exhibiting high negative reflectivity, low Poisson's ratio, high local continuity, and occurring near the top of an anticlinal fold. For an unconventional shale reservoir such as the Barnett Shale, such a correlation may be a pattern of laterally continuous brittle and ductile layers that correspond to the cyclicity of the Fort Worth Basin evolution, interrupted by faults and collapse features associated with the deeper Ellenburger dolomite.

The SOM (Kohonen, 1982) is one of the most popular seismic facies analysis algorithms that projects N-dimensional multiattribute data vectors, one for each voxel, onto a deformed lower dimensional surface that attempts to best fit the data distribution. Poupon et al. (1999) describe one of the earliest SOM-based seismic facies analyses. In their application, the attributes consisted of seismic amplitude from a suite of 16 phantom horizon slices. Data vectors in this 16D space were then projected onto a 1D shoestring "manifold" that best represented the data. The mean of each cluster along this shoestring therefore could be interpreted as a 16-sample seismic waveform. They then subsequently plotted the location of the cluster center along the 1D manifold against a 1D rainbow colorbar to delineate multiple tur-

[1]The University of Oklahoma, ConocoPhillips School of Geology and Geophysics, Norman, Oklahoma, USA. E-mail: tao-zhao@ou.edu; fangyu.li@ou.edu; kmarfurt@ou.edu.

Manuscript received by the Editor 8 August 2016; revised manuscript received 14 November 2016; published online 10 February 2017. This paper appears in *Interpretation*, Vol. 5, No. 2 (May 2017); p. T163–T171, 16 FIGS.

http://dx.doi.org/10.1190/INT-2016-0132.1.

bidite deposits. Later, Strecker and Uden (2002) cluster volumetric attributes such as envelope, frequency, and coherence rather than amplitudes extracted about a surface and project them onto a 2D deformed surface (manifold) rather than a 1D shoestring, plotting the cluster centers against a continuous 2D color table. Coléou et al. (2003) further this work using more sophisticated attributes. More recently, Matos et al. (2009) use concepts of intercluster distances and a 2D Hue, lightness, saturation (HLS) color table to improve the visualization of SOM facies. Roden et al. (2015) show how to incorporate PCA to select the most mathematically meaningful input attributes for SOM. Because the traditional Kohonen SOM only preserves topology but not distance, the distance information in the input attribute space is lost once projected into the 2D SOM latent space. Here, the "distance" is not the spatial/temporal distance defined in (x, y, and z) space in which the interpreter lives but rather the mathematical L_2 norm between two N-dimensional data vectors or between an N-dimensional data vector and an N-dimensional cluster center. Based on this definition, two data vectors that have a similar seismic-attribute response should be adjacent to each other, whereas their projections onto the deformed 2D manifold should also be close. To preserve the consistency of distance from input attribute space to 2D SOM space, Zhao et al. (2016) adopt a distance-preserving step, constraining the SOM facies to better reflect the degree of diversity as found in the input attribute space. However, unless the interpreter provides attributes that somehow measure the spatial proximity between two data vectors, the analysis remains spatially and temporally unaware.

The pitfall in being spatially and temporally unaware is the potential of mixing geology across different formations during the SOM process. In practice, an experienced interpreter can mitigate the possibility of mixing data samples from different formations by manipulating an operation window just localized at the target formation, yet there would always be vertical variations defined by sedimentary cycles in a different scale (ranges from hundreds of millions of years to one-tenth of a million years), e.g., pinchouts and thin layers, within the operation window. Adding information of stratigraphy (sedimentary cycle), which provides temporal (or spatial, if seismic data are in the depth domain) constraint on the vertical axis, may help to define layers that are otherwise not well-defined on seismic attributes. Relative geologic-time (RGT) volume generated from unwrapping instantaneous phase (Stark, 2003, 2004; Wu and Zhong, 2012) is an appropriate candidate for constraining SOM facies analysis with geologic time. However, in such RGT volumes, the vertical axis is monotonically increasing, on which sedimentary cycles controlled by changing sea level are not easily identified. In fact, there is very limited published research, if any, on calibrating RGT volumes with wells to identify sedimentary cycles that are routinely interpreted on well logs (e.g., gamma ray logs). An oscillation curve that directly links to periodic change in grain size is more preferred, and due to the limited resolution, presence of noise, and layer-interface relation in seismic data, such periodic change in grain size in most cases cannot be matched to seismic events. Empirical mode decomposition (EMD) (Huang et al., 1998) is an effective method to decompose seismic signal into several band-limited modes, and researchers have discovered that some of the decomposed modes (which are called intrinsic mode functions [IMFs]) corresponded with sedimentary cycles derived from well logs (Liu et al., 2010, 2015). However, EMD is a recursive decomposition method, and it is sensitive to noise and sampling and therefore not so robust. To overcome this issue, Dragomiretskiy and Zosso (2014) propose a novel mode decomposition method, variational mode decomposition (VMD), which decomposes a signal concurrently and is robust to noise and sampling. Lateral consistency-preserved VMD has been successfully applied to seismic amplitude data to derive a sedimentary cycle model (Li et al., 2016). In this study, we adopt the workflow described in Li et al. (2016) to derive a sedimentary cycle model, and we use this model as a constraint on SOM facies analysis. We test the proposed stratigraphy constrained SOM to a Barnett Shale survey in the United States, with the objective of recovering more subtle lithologic variations than using the unconstrained SOM.

We begin our paper by introducing the workflow of stratigraphy-constrained SOM, followed by the geologic background of the study area, which is in the Fort Worth Basin, United States. We then apply the stratigraphy-constrained SOM to analyze the lithofacies distribution in the Barnett Shale reservoir intervals. To illustrate the effectiveness of the proposed method, we also compare with the unconstrained SOM using the same input attributes. Finally, we summarize the values and limitations of the proposed method in the "Conclusion" section.

Stratigraphy-constrained SOM

The proposed method starts from extracting VMD modes (IMFs) from seismic amplitudes to build a sedimentary cycle model. In this implementation, we choose to decompose the seismic signal into four modes, aiming to represent the sedimentary cycles with varies orders. Because the IMFs are decomposed from seismic amplitude signal, which is the response of the interfaces, we further calculate the gradient of IMFs, assuming that the oscillation in the IMF gradients is a more suitable candidate to match with the sedimentary cycle caused by cyclic sea-level change, comparing with the oscillation of IMFs. To verify this assumption and choose the appropriate gradient, we use gamma ray logs as the representation of the sedimentary cycle pattern, and we compare with the derived IMF gradients to choose one that matches the gamma ray pattern the best. Such an IMF gradient with the highest correlation to the gamma ray log (referred in the later text as best

matching IMF gradient) is the sedimentary cycle model to be used to constrain the SOM.

In traditional Kohonen SOM, the distance used to find the best matching unit for a given multiattribute data sample vector is calculated using only attribute values. As discussed in the "Introduction" section, the lack of a temporal/spatial constraint may sometimes lead to unreasonable classification results. As an improvement, we add a term defined by the best matching IMF gradient into the distance metric, which now becomes

$$d = (1-\lambda)\sum_{i=1}^{N}\|\mathbf{a}_i - \hat{\mathbf{a}}_i\| + \lambda\|g - \hat{g}\|, \qquad (1)$$

where d is the weighted distance between a multiattribute data sample and a prototype vector, N is the number of attributes, $\mathbf{a}$ and $\hat{\mathbf{a}}$ are the N-dimensional multiattribute vectors at each voxel and of prototype vector, respectively, g and $\hat{g}$ are the best matching IMF gradients for a data sample and a prototype vector, respectively, and λ is a weight between zero and one.

Unfortunately, the weight λ is handpicked by interpreters. A larger weight means the generated SOM facies will follow the trend of IMF gradient more, and vice versa. A weight that is too large will generate a SOM facies map that follows the IMF gradient strictly and therefore suppress the response found in input attributes. A weight that is too small will not add the amount of constraint interpreters need. Therefore, an optimal weight is really up to the interpreter's choice and depends on project objective. In practice, we find that values of λ between 0.6 and 0.7 to provide good results. When $\lambda = 1/N + 1$, the IMF gradient is weighted equally with other attributes. Such a modification, although in an extremely simple form, introduces a degree of stratigraphic constraint, which we will later illustrate through our application. The complete workflow of the modified SOM facies analysis is shown in Figure 1.

Geologic setting

The seismic data used to evaluate the stratigraphy constrained SOM were acquired to image the Barnett Shale unconventional reservoir of the Fort Worth Basin, United States. The Fort Worth Basin is a shallow north–south-elongated foreland basin that encompasses roughly 15,000 mi^2 in north-central Texas and was formed during the late Paleozoic Ouachita orogeny (Walper, 1982). Being one of the most classic unconventional shale reservoir, the Barnett Shale is an organic-rich petroliferous shale formation deposited in Mississippian age, when an alternating series of black, organic-rich shales, and shallow marine limestones were deposited (Montgomery et al., 2005). The Barnett Formation is deposited directly over the Viola Limestone Formation, and topped by the Marble Falls Limestone Formation. In the study area, the Barnett Shale is further divided into an upper and lower interval by a limestone interval, known as the Forestburg Limestone (Montgomery et al., 2005). All three limestone intervals are water bearing and behave as highly ductile, which make them hydraulic fracturing barriers. The general stratigraphy of the Barnett Shale is shown in Figure 2. The upper and lower Barnett Shale formations are not homogeneous, and they can be subdivided into siliceous shale, argillaceous shale, calcareous shale, and limestone layers, with the presence of dolomite (Singh, 2008). Lithofacies-stacking patterns (usually systematic) are also identified in the Barnett Shale, which are controlled by the eustatic sea-level change over multiple scales of geologic time (Slatt and Abousleiman, 2011). Slatt and Abousleiman (2011) further define brittle-ductile couplets at different scales from such systematic lithofacies patterns identified on gamma ray logs and core cuttings, ranging from more than 100 m thick to only a few centimeters thick. The lithofacies patterns and brittle-ductile couplets are directly linked to sedimentary cycles that are a result of eustatic sea-level change. Therefore, if we are able to replicate the sedimentary cycles on seismic data and use such stratigraphic pattern to constrain the SOM analysis process, it well definitely benefit the facies classification, even though the sedimentary cycles are of high order due to the limited frequency band in seismic data.

Application

We applied the proposed stratigraphy constrained SOM facies analysis to the aforementioned Barnett Shale seismic survey, and we compared the facies analysis result with one from unconstrained SOM, using the same input attributes and model parameters. In unconventional shale reservoirs, in which interpreters are usually interested in lithology changes more than structural deformations, we prefer seismic inversion attrib-

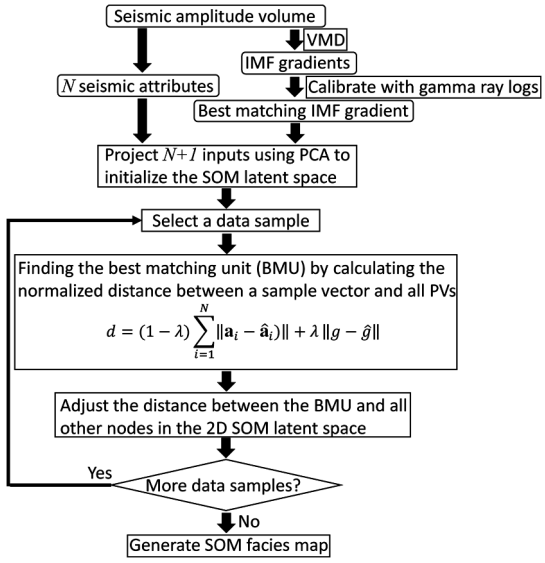

Figure 1 Workflow of the stratigraphy constrained SOM facies analysis. All abbreviations are explained in the main text.

utes as the input attributes for automatic facies analysis algorithms. Zhang et al. (2015b) and Verma et al. (2016) use such inversion attributes to estimate brittleness and total organic carbon in a supervised fashion. Spectral decomposition attributes are also routinely used as lithology indicators, and they are especially helpful in mapping the horizontal extension of different facies and geobodies. However, due to the window-based nature when generating such attributes, spectral decomposition attributes, such as peak spectral frequency and magnitude, have suboptimal vertical resolution; therefore, they are not suitable to represent vertical stacking patterns resulted from cyclic sea-level change. In this study, attributes from prestack simultaneous inversion were used as inputs, which are P-impedance Z_P, S-impedance Z_S, the ratio of incompressibility and shear modulus λ/μ, and Poisson's ratio ν. We selected these attributes with the understanding that such attributes directly correlate with mineral contents, grain size, and elastic properties of the rocks. The prestack seismic data were carefully processed and preconditioned with the workflow described by Zhang et al. (2013, 2015a).

With the input attributes at our disposal, the next step is to generate the four IMFs using VMD. Figure 3 shows an example trace along well A (location shown in later figures) together with its decomposed four IMFs, and the gradient of IMF 3, which, after further analysis, was able to match the pattern found in gamma ray logs. Figure 4 shows the vertical sections along the seismic amplitude and the gradient of IMF 3 plotted with the gamma ray log at well A, and Figure 5 shows how the composite trace of the gradient of IMF 3 matches the gamma ray log along wells A and B (locations of both wells are shown in later figures). In Figure 4, formation tops are marked as solid colored curves, gamma ray logs as a solid blue curve, and the well trajectory as a dashed red line. From the top to the bottom, the marked formation tops are Marble Falls Limestone, Upper Barnett Limestone, Upper Barnett Shale, Forestburg Limestone, and Lower Barnett Shale. The formation tops are displayed in the same color scheme for all remaining figures. We identify a similar cyclic pattern in the IMF 3 gradient as in the gamma ray log, which is commonly used by sequence stratigraphers to interpret sedimentary cycles controlled by eustatic sea-level change, subsidence rate of the basin, and sediment supply. Therefore, the gradient of IMF 3 provides a volumetric approximation of sedimentary

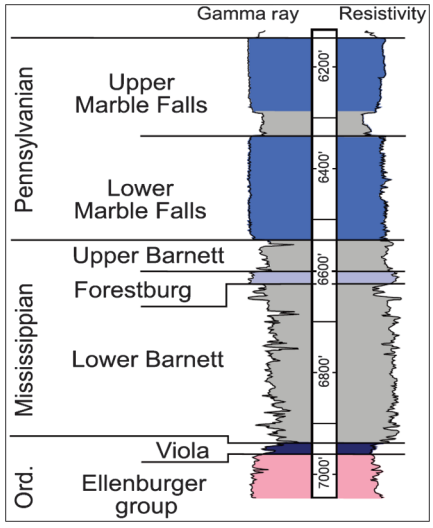

Figure 2 General stratigraphy of the Ordovician to Pennsylvanian section in the Fort Worth Basin through a well near the study area (after Loucks and Ruppel, 2007).

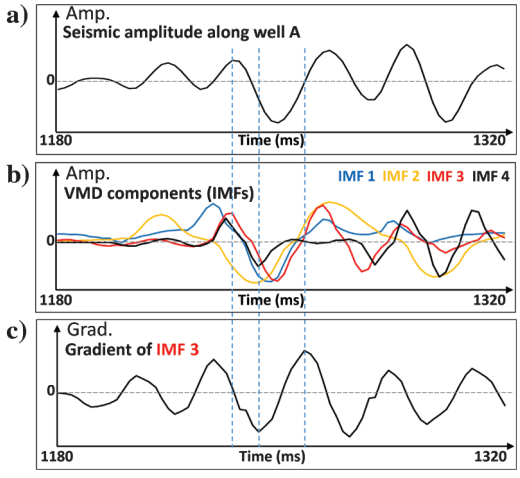

Figure 3 (a) Seismic amplitude from a trace along well A (location shown in Figure 6). (b) VMD components (IMFs) of the trace above. Four components are used to represent sedimentary cycle at different scales. (c) The gradient of IMF 3. The dashed lines show the correspondence among seismic amplitude, IMF 3, and IMF 3 gradient, when IMF 3 gradient is at zero, local minimum, and local maximum.

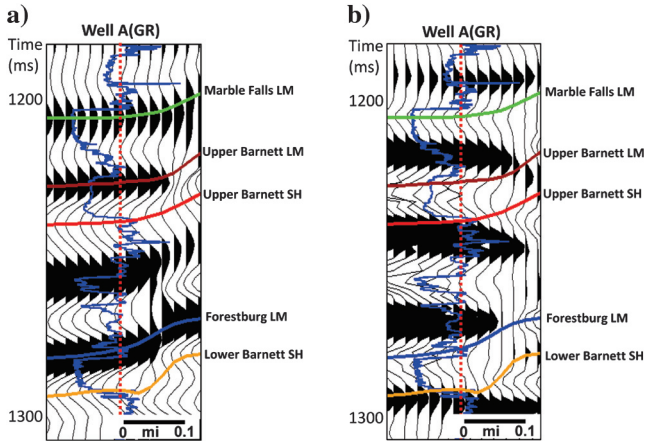

Figure 4 Vertical sections along the seismic amplitude and IMF 3 gradient plotted with the gamma ray log (blue curve) at well A (location shown in Figure 6). The well trajectory is marked by the red dashed line. Formation tops are marked as colored curves. Note the good match in patterns between the gamma ray log and IMF 3 gradient.

cycles, providing information that is not easily acquired from traditional spectral decomposition.

We provided the input attributes with and without the constraint to a SOM classifier defined in the workflow discussed in Figure 1. Figure 6 shows time slices from unconstrained SOM (Figure 6a) and constrained SOM (Figure 6b), on which the location of wells A and B and vertical sections AA′, BB′, and CC′ (discussed later) are displayed. The facies maps are generated by crossplotting the data projected onto two SOM axes, and such a crossplot enables the use of a 2D color map, providing better visualization. By looking at these two time slices alone, it is nearly impossible to draw any conclusions comparing the quality of facies because the contribution of the stratigraphy constraint is in the vertical direction. Moving to the vertical section AA′, Figure 7 shows the unconstrained SOM facies, and Figure 8 shows the constrained SOM facies, both of which are overlapped by the gamma ray log at well B. The formation tops are marked as colored curves. We identify the gamma ray value increases from the top to the bottom in the Marble Falls Limestone (black arrows in Figures 7 and 8), which translates into a color change from purplish to magenta in the unconstrained SOM facies (Figure 7), and a color change from orange to lime green in the constrained SOM facies (Figure 8). Adding the stratigraphy constraint makes such lithology variation more obvious in the form of colors with higher contrast, and matches the gamma ray trend better. The white arrows in Figures 7 and 8 show a local variation within the Upper Barnett Formation, which is more obvious on the constrained SOM facies. Figure 9 displays vertical section AA′ along with the V_P/V_S ratio. Although V_P/V_S is derived from Z_P and Z_S, it is not directly used as an input attribute for SOM. We clearly identify a high V_P/V_S ratio layer corresponding to the high gamma ray at the bottom of Marble Falls Limestone, and a very low V_P/V_S zone within the Upper Barnett at the white arrow.

Figures 10 and 11 are the vertical sections of unconstrained and constrained SOM facies maps along line BB′, respectively. Here, besides the higher color contrast at the Marble Falls Limestone and Upper Barnett Limestone, the constrained SOM also shows more details in the Upper Barnett Shale formation, compared to the unconstrained SOM. As previously discussed, the Barnett Shale is deposited over multiple cycles of sea-level change, and thin layers at different scales are developed. In the unconstrained SOM facies map (Figure 10), the middle section of the Upper Barnett Shale is a thick layer of grayish colors, with a hint of yellow. However, in the same region of the constrained SOM facies map (Figure 11), the two black arrows point

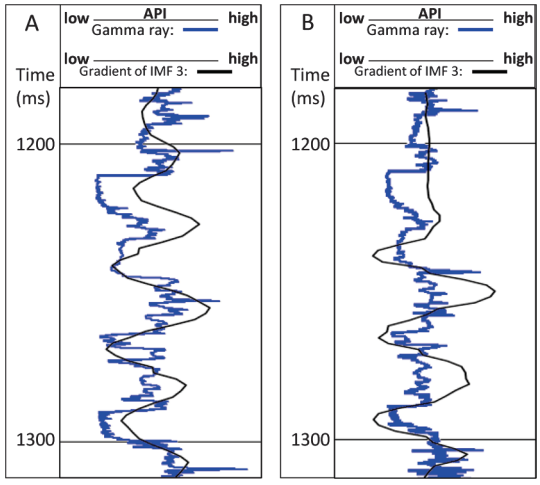

Figure 5 Traces of IMF 3 gradient plotted with gamma ray logs (blue curve) at well A (left) and well B (right) (well locations are shown in Figure 6). Well A is a vertical well, and the corresponding IMF 3 gradient trace is the most adjacent trace of well A. Well B is a deviated well, and the corresponding IMF 3 gradient trace is a composite trace along the well trajectory. Note the good match in pattern between the gamma ray log and IMF 3 gradient at both wells.

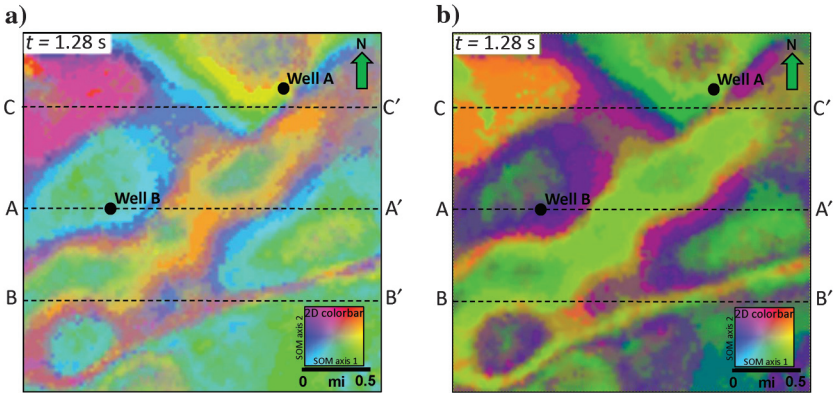

Figure 6 Time slices at $t = 1.28$ s along SOM facies maps generated (a) without stratigraphy constraint and (b) with stratigraphy constraint. A 2D colorbar is used for visualization. Note the difference between two time slices is very limited because the stratigraphy constraint is added on the vertical axis.

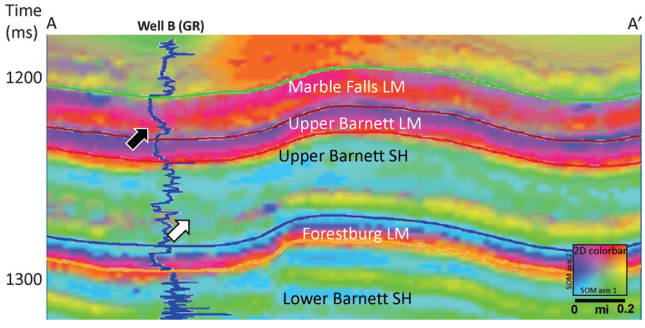

Figure 7 Vertical section along line AA′ (location shown in Figure 6) through unconstrained SOM facies map. Formation tops are marked with colored curves. The black arrow indicates a high gamma ray layer at the bottom of the Marble Falls Limestone formation. The white arrow indicates a local facies change.

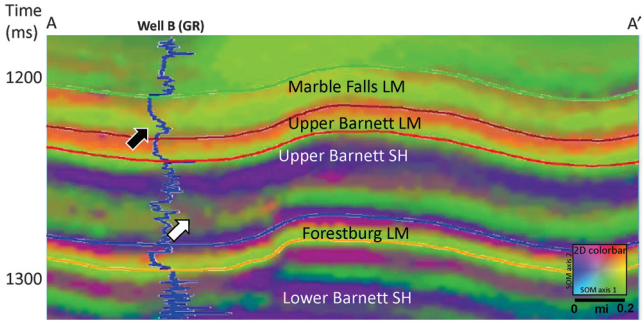

Figure 8. Vertical section along line AA′ (location shown in Figure 6) through constrained SOM facies map. Formation tops are marked with colored curves. The black arrow indicates a high-gamma-ray layer at the bottom of the Marble Falls Limestone formation. This high-gamma-ray layer corresponds better to the constrained SOM facies than the unconstrained SOM facies, as the facies show higher contrast in color (orange to lime versus purple to magenta in Figure 7). The white arrow indicates a local facies change in the Upper Barnett, which corresponds to a low V_P/V_S region.

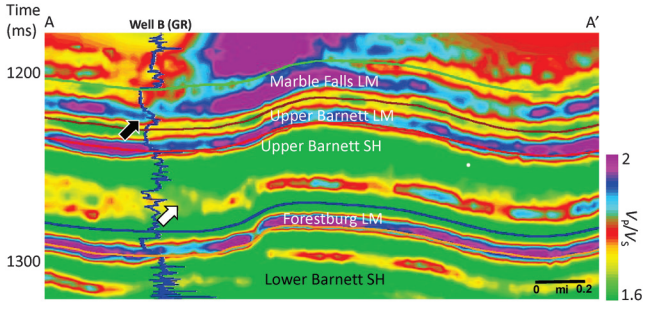

Figure 9. Vertical section along line AA′ (location shown in Figure 6) through V_P/V_S ratio. Formation tops are marked with colored curves. The black arrow indicates a high-gamma-ray layer at the bottom of the Marble Falls Limestone formation. This high-gamma-ray layer has a very high V_P/V_S ratio. The white arrow indicates a low V_P/V_S region.

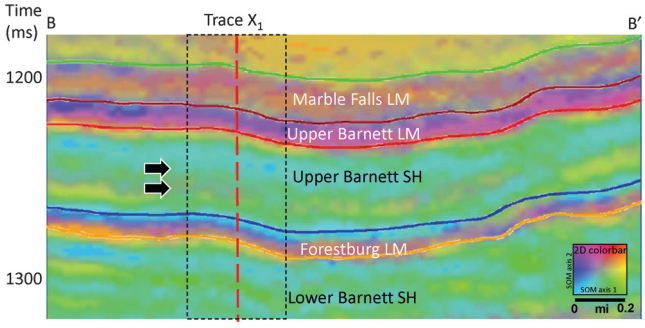

Figure 10. Vertical section along line BB′ (location shown in Figure 6) through the unconstrained SOM facies map. Formation tops are marked with colored curves. The black arrows indicate two thin layers in the Upper Barnett Shale formation that are not well-defined in the unconstrained SOM facies map. The area in the dashed box is discussed in Figure 13. The red dashed line is the location of trace X_1, which is discussed in Figure 13.

at two facies with different colors in a stacking pattern, which are nearly identical in Figure 10. Figure 12 shows that a vertical section of the V_P/V_S ratio along the same BB′ line, which does not contain the sedimentary cycle information, can still provide an indication of thin layers of different V_P/V_S ratio, and the green facies in Figure 11 clearly correlates with the relatively higher V_P/V_S regions in the middle part of Upper Barnett Shale. Figure 13 shows a magnification around traces X_1 and X_1' that are extracted from the unconstrained and constrained SOM facies volumes, respectively, at the same location and overlaid with a curve display of these two traces. The values on the traces are "facies numbers," which are overdefined with 4096 SOM prototype vectors to ensure a smooth visualization. Such 4096 "facies" are then arranged over a 64×64 2D space, and color coded using the 2D color map shown in the lower right corner. This translates to the fact that facies N and facies $N \pm 64$ have similar colors, so the curve

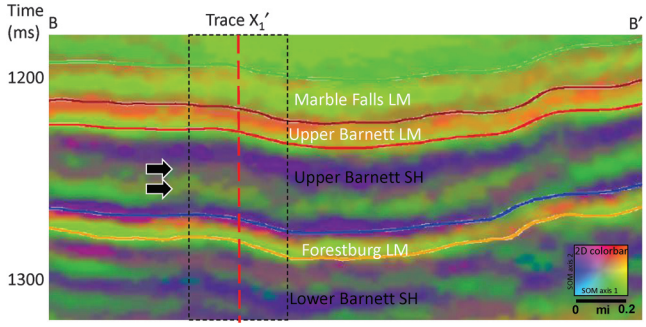

Figure 11 Vertical section along line BB′ (location shown in Figure 6) through the constrained SOM facies map. Formation tops are marked with colored curves. The black arrows indicate two thin layers in the Upper Barnett Shale formation that can be identified in the constrained SOM facies map but are not well-defined in the unconstrained SOM facies map. The area in the dashed box is discussed in Figure 13. The red dashed line is the location of trace X_1', which is discussed in Figure 13.

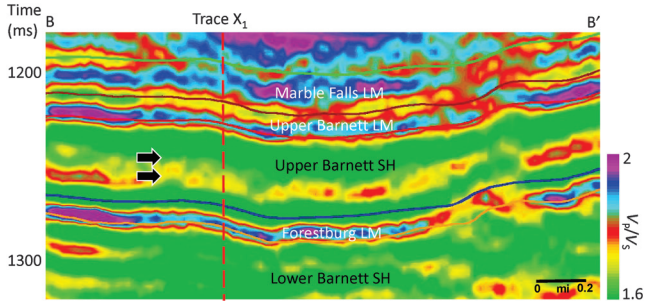

Figure 12 Vertical section along line BB′ (location shown in Figure 6) through V_P/V_S ratio. Formation tops are marked with colored curves. The black arrows indicate two thin layers in the Upper Barnett Shale formation identified in the constrained SOM facies map. Although the stratigraphy constrain is not from the V_P/V_S ratio, we do observe a difference in the V_P/V_S ratio between these two layers. The red dashed line is the location of trace X_1/X_1', which is discussed in Figure 13.

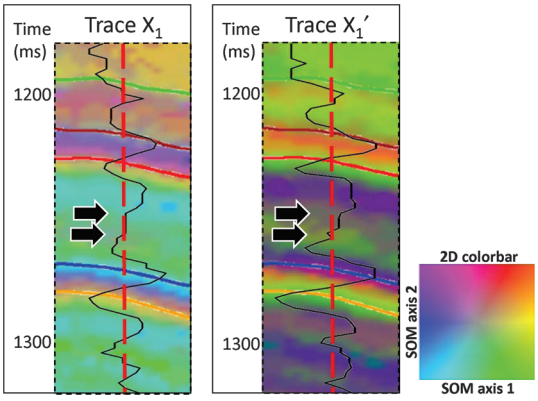

Figure 13 Magnified around traces X_1 and X_1' extracted from the unconstrained and constrained SOM facies volume, respectively, at the same location, and overlaid with curve display of these two traces. The values on the traces are facies numbers, which are overdefined with 4096 SOM prototype vectors to ensure a smooth visualization. Such 4096 facies are then arranged over a 64×64 2D space, and color coded using the 2D color map shown in the lower right corner. We identify different layers (black arrows) on trace X_1', but they are nearly impossible to see on trace X_1.

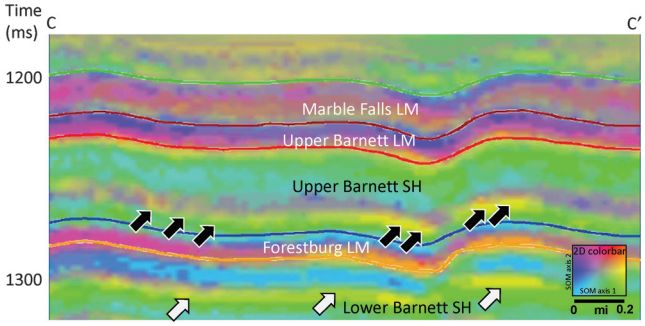

Figure 14. Vertical section along line CC′ (location shown in Figure 6) through the unconstrained SOM facies map. Formation tops are marked with colored curves. The black arrows indicate a thin layer with a high V_P/V_S ratio in the Upper Barnett Shale formation. The white arrows indicate a thin layer with a high V_P/V_S ratio in the Lower Barnett Shale formation.

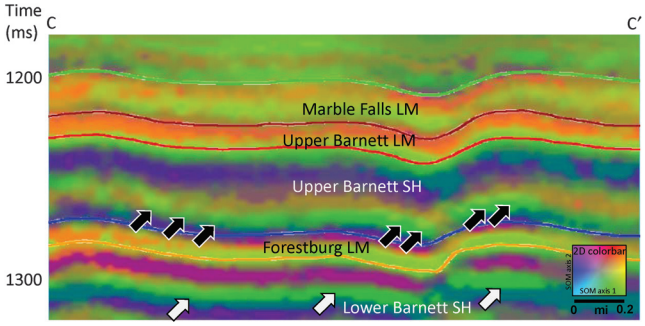

Figure 15. Vertical section along line CC′ (location shown in Figure 6) through the constrained SOM facies map. Formation tops are marked with colored curves. The black arrows indicate a thin layer with high V_P/V_S ratio in the Upper Barnett Shale formation. The white arrows indicate a thin layer with high V_P/V_S ratio in the Lower Barnett Shale formation.

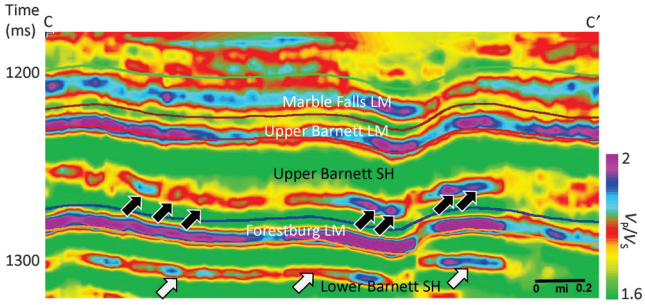

Figure 16. Vertical section along line CC′ (location shown in Figure 6) through the V_P/V_S ratio. Formation tops are marked with colored curves. The black arrows indicate a thin layer with high V_P/V_S ratio in the Upper Barnett Shale formation. The white arrows indicate a thin layer with high V_P/V_S ratio in the Lower Barnett Shale formation.

display alone may sometime be misleading and has to be verified with a color display. In practice, we are still able to see different layers (black arrows) on trace X_1', but it is nearly impossible to see on trace X_1. Such details provide interpreters more insights of the small scale stratigraphy distribution in the Upper Barnett Shale formation.

Figures 14, 15, and 16 show the unconstrained SOM facies, constrained SOM facies, and V_P/V_S ratio along line CC′, respectively. Similar to line AA′ and BB′, we are still able to identify more facies with higher color contrast in the constrained SOM facies, whereas in the unconstrained SOM facies map, the facies are more smeared. The black arrows point to some high V_P/V_S regions in the Upper Barnett formation, which are better delineated in the constrained SOM map as bright green spots (Figure 15). The constrained SOM map also shows the high V_P/V_S layer in the Lower Barnett (white arrows) clearer than in the unconstrained SOM map. Better delineation of such local elastic property change will greatly facilitate well planning in the completion stage.

Conclusions

We explored the feasibility of constraining the SOM facies analysis using stratigraphy information, in the form of sedimentary cycles. The stratigraphy constrained SOM facies map provides more details and shows layers that are more likely being overlooked on SOM facies maps without such constraints. The extra features can be calibrated with well log data and the V_P/V_S ratio attribute, which prove the credibility of the resulted facies. The sedimentary cycle is estimated by decomposing seismic amplitude signal into a finite number of modes using VMD, and we believe the selection of the most appropriate component to represent sedimentary cycle requires calibration with other data, and the most appropriate component may differ from region to region. However, the geologic meaning of such modes is not well understood, and these modes need to be carefully calibrated with well logs. The different VMD gradient patterns in adjacent

layers are a good indicator of layer geometry; however, layers with the same VMD gradient response are not distinguishable. Fortunately, such a limitation poses less of a problem in real application because adjacent layers rarely have the same VMD gradient in the seismic scale.

Acknowledgments

We thank Devon Energy for providing the seismic and well log data. Financial support for this effort is provided by the industry sponsors of the Attribute-Assisted Seismic Processing and Interpretation (AASPI) consortium at the University of Oklahoma. The prestack inversion was performed using licenses to Hampson and Russell provided to the University of Oklahoma for research and education courtesy of CGG GeoSoftware, and all visualizations are from Petrel, courtesy of Schlumberger.

References

Coléou, T., M. Poupon, and K. Azbel, 2003, Unsupervised seismic facies classification: A review and comparison of techniques and implementation: The Leading Edge, **22**, 942–953, doi: 10.1190/1.1623635.

Dragomiretskiy, K., and D. Zosso, 2014, Variational mode decomposition: IEEE Transactions on Signal Processing, **62**, 531–544.

Huang, N. E., Z. Shen, S. R. Long, M. C. Wu, H. H. Shih, Q. Zheng, N.-C. Yen, C. C. Tung, and H. H. Liu, 1998, The empirical mode decomposition and the Hilbert spectrum for nonlinear and nonstationary time series analysis: Proceedings of the Royal Society of London A: Mathematical, Physical and Engineering Sciences, The Royal Society, **454**, 903–995, doi: 10.1098/rspa.1998.0193.

Kohonen, T., 1982, Self-organized formation of topologically correct feature maps: Biological Cybernetics, **43**, 59–69, doi: 10.1007/BF00337288.

Li, F., T. Zhao, X. Qi, K. Marfurt, and B. Zhang, 2016, Lateral consistency preserved variational mode decomposition (VMD): 86th Annual International Meeting, SEG, Expanded Abstracts, 1717–1721, doi: 10.1190/segam2016-13880188.1.

Liu, Q., W. Yang, and L. Tian, 2010, Research and application of seismic facies analysis based on the empirical mode decomposition: 80th Annual International Meeting, SEG, Expanded Abstracts, 2329–2333.

Liu, Y., G. Yang, and W. Cao, 2015, The division of sedimentary cycle based on HHT: 85th Annual International Meeting, SEG, Expanded Abstracts, 1902–1906.

Loucks, G. R., and C. S. Ruppel, 2007, Mississippian Barnett shale: Lithofacies and depositional setting of a deep-water shale-gas succession in the Fort Worth Basin, Texas: AAPG Bulletin, **91**, 579–601, doi: 10.1306/11020606059.

Matos, M. C., K. J. Marfurt, and P. R. S. Johann, 2009, Seismic color self-organizing maps: Presented at the 11th International Congress of the Brazilian Geophysical Society, Extended Abstracts.

Montgomery, S. L., D. M. Jarvie, K. A. Bowker, and R. M. Pollastro, 2005, Mississippian Barnett shale, Fort Worth basin, north-central Texas: Gas-shale play with multi-trillion cubic foot potential: AAPG Bulletin, **89**, 155–175, doi: 10.1306/09170404042.

Poupon, M., K. Azbel, and G. Palmer, 1999, A new methodology based on seismic facies analysis and litho-seismic modeling: The Elkhorn Slough field pilot project, Solano County, California: 69th Annual International Meeting, SEG, Expanded Abstracts, 927–930.

Roden, R., T. Smith, and D. Sacrey, 2015, Geologic pattern recognition from seismic attributes: Principal component analysis and self-organizing maps: Interpretation, **3**, no. 4, SAE59–SAE83, doi: 10.1190/INT-2015-0037.1.

Singh, P., 2008, Lithofacies and sequence stratigraphic framework of the Barnett shale, Northeast Texas: Ph. D. dissertation, University of Oklahoma.

Slatt, R. M., and Y. Abousleiman, 2011, Merging sequence stratigraphy and geomechanics for unconventional gas shales: The Leading Edge, **30**, 274–282, doi: 10.1190/1.3567258.

Stark, T. J., 2003, Unwrapping instantaneous phase to generate a relative geologic time volume: 73rd Annual International Meeting, SEG, Expanded Abstracts, 1707–1710.

Stark, T. J., 2004, Relative geologic time (age) volumes — Relating every seismic sample to a geologically reasonable horizon: The Leading Edge, **23**, 928–932.

Strecker, U., and R. Uden, 2002, Data mining of 3D poststack attribute volumes using Kohonen self-organizing maps: The Leading Edge, **21**, 1032–1037, doi: 10.1190/1.1518442.

Verma, S., T. Zhao, K. J. Marfurt, and D. Devegowda, 2016, Estimation of total organic carbon and brittleness volume: Interpretation, **4**, no. 3, T373–T385, doi: 10.1190/INT-2015-0166.1.

Walper, J. L., 1982, Plate tectonic evolution of the Fort Worth basin, *in* C. A. Martin, ed., Petroleum geology of the Fort Worth basin and Bend arch area: Dallas Geological Society, 237–251.

Wu, X., and G. Zhong, 2012, Generating a relative geologic time volume by 3D graph-cut phase unwrapping method with horizon and unconformity constraints: Geophysics, **77**, no. 4, O21–O34, doi: 10.1190/geo2011-0351.1.

Zhang, B., D. Chang, T. Lin, and K. J. Marfurt, 2015a, Improving the quality of prestack inversion by prestack data conditioning: Interpretation, **3**, no. 1,T5–T12, doi: 10.1190/INT-2014-0124.1.

Zhang, B., K. Zhang, S. Guo, and K. J. Marfurt, 2013, Nonstretching NMO correction of prestack time-migrated gathers using a matching-pursuit algorithm: Geophysics, **78**, no. 4, U9–U18, doi: 10.1190/geo2011-0509.1.

Zhang, B., T. Zhao, X. Jin, and K. J. Marfurt, 2015b, Brittleness evaluation of resource plays by integrating petro-

physical and seismic data analysis: Interpretation, **3**, no. 2, T81–T92, doi: 10.1190/INT-2014-0144.1.

Zhao, T., V. Jayaram, A. Roy, and K. J. Marfurt, 2015, A comparison of classification techniques for seismic facies recognition: Interpretation, **3**, no. 4, SAE29–SAE58, doi: 10.1190/INT-2015-0044.1.

Zhao, T., J. Zhang, F. Li, and K. J. Marfurt, 2016, Characterizing a turbidite system in Canterbury Basin, New Zealand, using seismic attributes and distance-preserving self-organizing maps: Interpretation, **4**, no. 1, SB79–SB89, doi: 10.1190/INT-2015-0094.1.

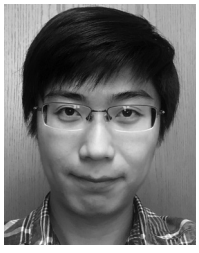

Tao Zhao received a B.S. (2011) in exploration geophysics from the China University of Petroleum and an M.S. (2013) in geophysics from the University of Tulsa. He is currently pursuing a Ph.D. in geophysics at the University of Oklahoma as a member of the Attribute Assisted Seismic Processing and Interpretation (AASPI) consortium. His current research interests include developing and applying pattern recognition and machine learning techniques in seismic facies analysis, unconventional shale resource play characterization, and seismic attribute development.

Fangyu Li received a bachelor's degree (2009) in electrical engineering from Beihang University and a master's degree (2013) in electrical engineering from Tsinghua University. He is pursuing a Ph.D. in geophysics at the University of Oklahoma. His research interests include seismic processing, quantitative seismic interpretation, and seismic attribute development.

Kurt J. Marfurt received a Ph.D. (1978) in applied geophysics at Columbia University's Henry Krumb School of Mines in New York. He joined The University of Oklahoma in 2007 where he teaches geophysics. His career includes 18 years with Amoco Research and 20 years in academia. He teaches short courses on attributes for SEG and AAPG and currently serves as editor of *Interpretation*. His research interests include the development and calibration of new seismic attributes to aid in seismic processing, seismic interpretation, and reservoir characterization, with a focus on resource plays.